# A Wavenumber–Frequency Spectrum of Upper Ocean Shear

ROBERT PINKEL

*Marine Physical Laboratory, Scripps Institution of Oceanography, University of California, San Diego, La Jolla, CA 92093*

## ABSTRACT

In May 1980 an 18-day sequence of oceanic velocity profiles was obtained off the coast of Southern California. The measurements were made using a pair of Doppler sonars mounted on the research platform FLIP and angled downward 45°. The profiles extend to a depth of 600 m. Depth resolution is approximately 30 m. From these profiles the vertical wavenumber-frequency spectrum of the oceanic shear field, $\Phi(\kappa, \omega) \equiv \langle(\partial u/\partial z)^2\rangle/ d\kappa d\omega$ is estimated.

The shear spectrum is resolved between vertical wavenumbers 1/530 and 1/28 cpm. It is band-limited in wavenumber in the frequency region encompassing near-inertial waves and semidiurnal tides. Motions of vertical wavelength between 100 and 300 m have the greatest shear spectral density. As frequency increases, the band of most energetic motion shifts to ever higher wavenumbers. At frequencies above 8 cpd only the low-wavenumber side of the energetic band can be resolved by the sonars. The wavenumber dependence here appears blue.

It is unlikely that the high-frequency, high-wavenumber shear is a result of linear internal wave activity. The spectrum $\Phi(\kappa, \omega)$ is not consistent with previous estimates of the spectrum of isotherm vertical displacement if linear internal wave scaling is used. The vertical displacement spectrum becomes progressively more red (low-mode dominated) with increasing frequency while the shear spectrum becomes progressively more blue. In ignorance of the dynamics of these motions, it is unwise to use internal wave (WKB) scaling to describe the vertical variation of the shear field.

## 1. Introduction

This paper presents estimates of the vertical wavenumber–frequency spectrum of shear, $\Phi(\kappa, \omega)$. Measurements were made using a pair of Doppler sonar mounted on the Research Platform FLIP. The shear spectral estimates are essentially reweighted versions of velocity spectra presented in a companion paper (Pinkel, 1984). It is worthwhile to present them independently here in that they differ greatly from the preexisting model of the shear spectrum (Garrett and Munk, 1975, 1979). Specifically, at low frequency (one to three times inertial) the wavenumber dependence of the spectrum is band limited. The greatest variance density is associated with 100–300 m vertical scales. At higher frequencies the spectrum becomes progressively more blue (Figs. 1 and 2).

Two points will be emphasized in this work. The first is that this unusual estimate of $\Phi(\kappa, \omega)$ is completely consistent with previous estimates of the shear spectrum as a function of vertical wavenumber alone, $\Phi(\kappa)$. Specifically, Gargett *et al.* (1981) have presented estimates of $\Phi(\kappa)$ which are white down to scales of 10 m and change to a $\kappa^{-1}$ form between 10 and 1 m. When $\Phi(\kappa, \omega)$ is integrated over frequency, the resulting wavenumber spectrum is essentially white, at vertical scales less than 100 m. The finite (30 m) vertical resolution of the sonars precludes comparison with Gargett *et al.* (1981) at small scales.

The second point is that the high frequency–high vertical wavenumber shear variance, which is a significant fraction of the overall shear in the sea, is not likely due to linear internal waves. Previous estimates of the wavenumber–frequency spectrum of isotherm vertical displacement (Pinkel, 1975) have a high wavenumber–high frequency spectral form which is inconsistent with the present estimate of $\Phi(\kappa, \omega)$ if linear internal wave scaling is applied. Specifically, the wavenumber dependence of the displacement spectrum becomes more red with increasing frequency while that of the shear spectrum becomes more blue.

It is likely that the advection of motions of small horizontal scale by the larger scale flows contributes to this discrepancy. The advected features must have a high length-to-depth aspect ratio while simultaneously having a short horizontal length, to be consistent with the measurements. Whether these are internal waves of low intrinsic frequency or quasi-geostrophic features of very small scale, as suggested by Holloway (1983), is currently unclear.

A brief description of the measurements and the analysis technique is given next. The remainder of the paper discusses various forms of the shear spectrum that are presented.

## 2. Measurements

The observations of the shear field occurred during an 18-day period in May 1980. The measurements were made using a pair of Doppler sonars mounted on the
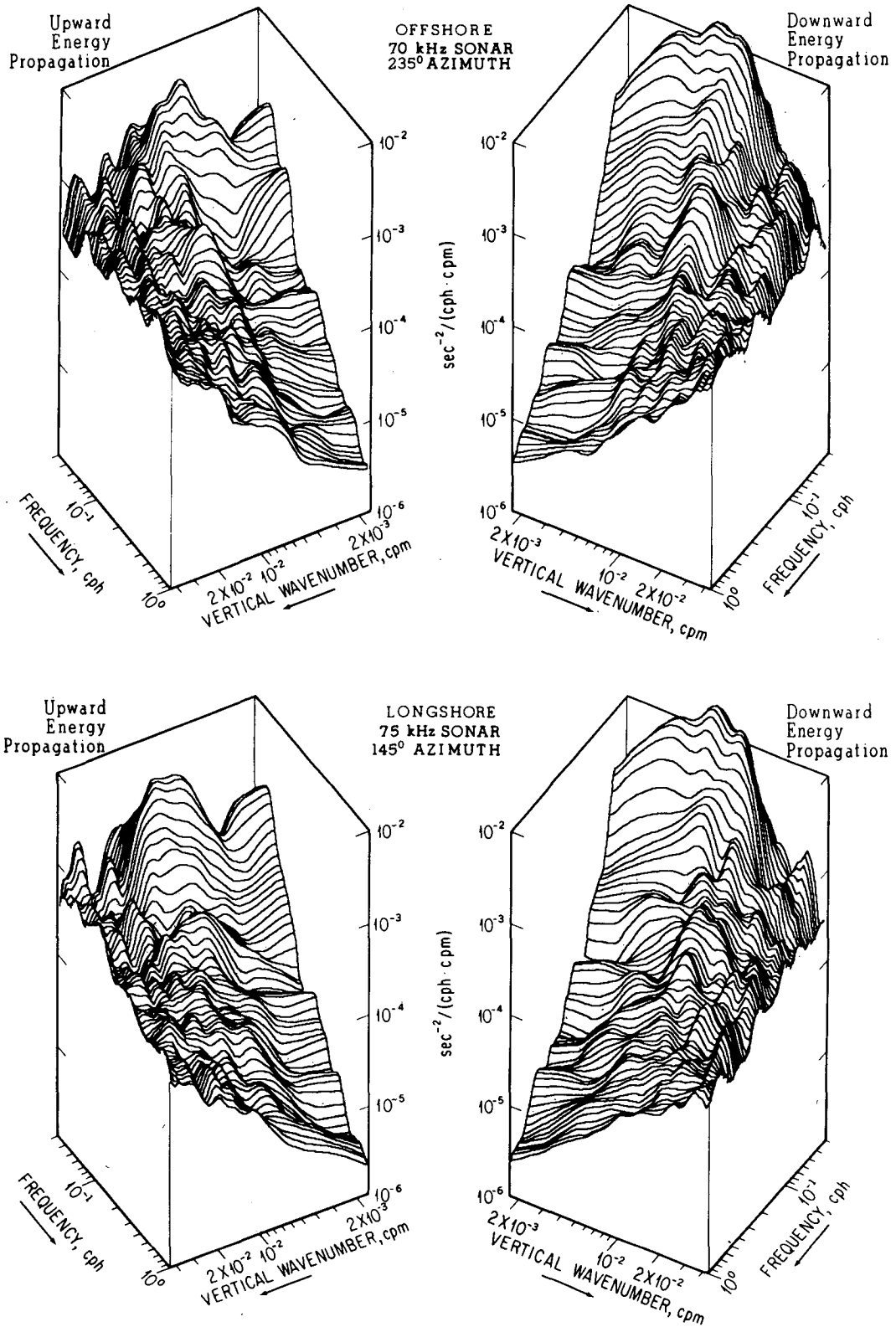
FIG. 1. Component wavenumber–frequency spectrum of shear for the 70- and 75-kHz sonars. A near-inertial peak dominates the spectrum at low frequency and wavenumber. At higher frequencies the wavenumber dependence of the spectrum becomes progressively more blue. No modeled noise is removed in this spectral estimate. The "noise correction" process has very little effect at frequencies below 1 cph.
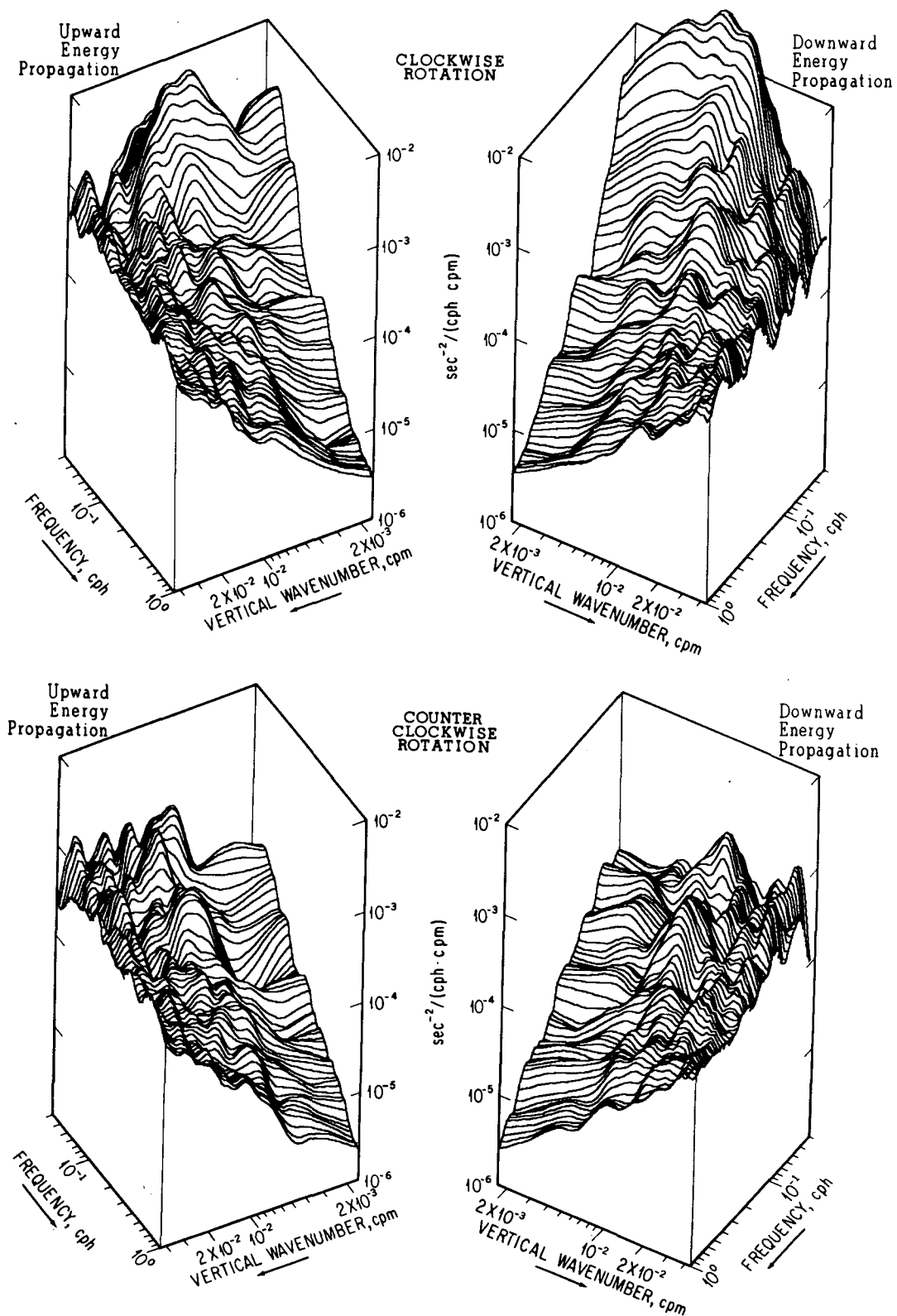
FIG. 2. Rotary wavenumber–frequency spectrum of shear. These estimates are obtained by combining information from the offshore and longshore sonars. No modeled noise is removed.

Research Platform FLIP. The operation commensed at 30°50'N, 124°0'W, approximately 500 km WSW of San Diego. It concluded 200 km to the south, at 28°40'N, 124°0'W.

The sonars were mounted on FLIP's hull at a depth of 38 m and slanted 45° downward. They were operated at frequencies of 70 and 75 kHz. The 70-kHz sonar was directed toward 235° true, a direction nearly orthogonal to the Patton Escarpment, a 2 km step in the seafloor which parallels the California coast for some 500 km. It will henceforth be referred to as the offshore sonar. The 75-kHz sonar was oriented toward 135° True, approximately parallel to the escarpment and (perhaps) to the mean path of the California Current. The strategy was to maximize the sensitivity of the offshore sonar to baroclinic motions generated at the Patton Escarpment by the barotropic tides. It was anticipated that the orthogonal, longshore sonar (75 kHz) would see the less of a tidal signature and more of the effects of the mean shear of the California Current. These measurements are described in greater detail by Pinkel (1983). The subsequent wavenumber–frequency spectral analysis is described by Pinkel (1984).

There are several significant technical uncertainties in this work. One consideration is the use of WKB stretching in the two-dimensional spectral analysis of these data. WKB stretching is used to correct for the effects of refraction of the propagating internal waves, due to variation of the Väisälä frequency with depth (Pinkel, 1984). It is seen below that a significant contribution to the shear variance comes from high-frequency motions that are not likely linear internal waves. The effect of the WKB stretching is to introduce a spatial nonhomogeneity to these motions. While this effect is probably slight, it is nevertheless a concern.

A second uncertainty is associated with measurement noise. The noise results predominantly from measurement errors in the sonars which are localized in space and time. The velocity noise spectrum should be white in frequency and wavenumber. The resulting shear-noise spectrum would then have a $\kappa^2$ wavenumber dependence. The issue is whether this noise dominates the spectrum of the water motion in any region of the frequency–wavenumber domain resolved by the experiment.

Simple modeling of the shear-noise spectrum suggests it will be a significant contributor in the high-frequency, high-wavenumber region. Fortunately, the effect of the noise contamination can be ascertained by subtracting a $\kappa^2$ spectrum of the appropriate level from the estimated shear spectrum. While simple to implement, this correction alters the estimate of overall shear variance. It also changes the wavenumber dependence of the spectrum at very high frequencies from a monotonically increasing form to a band-limited one.

To aid the reader in distinguishing those spectral regions that are unaffected by noise, those where the influence of noise is easily understood, and those where

there is no useful information, spectral estimates are presented in this paper both with and without the modeled noise removed. This enables an intuitive assessment of the data quality. A model shear-noise spectrum corresponding to a velocity noise level of 1.5 $cm^2$ $s^{-2}$ is used. This is somewhat less than the actual noise experienced in the offshore, 70-kHz measurements, but more than that experienced in the longshore, 75-kHz measurement. Fortunately, the essential conclusions of this work remain unaffected even when so much modeled noise is "removed" that the resulting longshore spectrum becomes negative at high wavenumber.

The dominant technical uncertainty in the work results from the tilting motion of FLIP. This not only degrades the vertical resolution of the measurements, but also confuses the depth and time dependence of the signals. Both effects are potentially significant, even given the very modest values of FLIP's tilt (0.5–2° rms at frequencies above 1 cpm, depending on sea state, 0.5° rms or less at frequencies below 1 cpm). A discussion of the effects of tilt, including model simulations, is presented in the Appendix. Artifacts associated with FLIP's motion are noted in the text.

The spectral analysis is described in detail by Pinkel (1984), and can be summarized briefly here. The velocity series are first differenced in both time and range and are then Fourier transformed in time. The resulting Fourier coefficients are WKB stretched and Fourier transformed in depth. To obtain spectral estimates of shear rather than "first differenced velocity" the squared Fourier coefficients are "recolored" in wavenumber using the factor $\{(\pi\kappa/\kappa_n)^2/[2 - 2\cos(\pi\kappa/\kappa_n)]\}$ where $\kappa$ is the wavenumber and $\kappa_n$ is the Nyquist wavenumber. This factor differs significantly from unity as the Nyquist wavenumber is approached, where it reaches the value $\pi^2/4$. The conventional factor $1/[2 - 2\cos(\pi\omega/\omega_n)]$ is used to recolor the frequency dependence of the spectrum.

Unlike as done by Pinkel (1984), the units of the shear spectra presented here have been scaled to give the variance of horizontal (not slant) velocity per unit of vertical (not slant) distance. Spectral density is given per cycle per vertical (not slant) meter. This facilitates direct comparison with the shear spectrum of Gargett et al. (1981). To justify this conversion, one must assume that the slant differences in vertical velocity are negligibly small and that the horizontal gradient of horizontal velocity is small compared to the vertical gradient (Appendix).

The shear spectrum $\Phi(\kappa, \omega)$ is presented in several different formats in this paper. In Fig. 1, deformed surface plots of the spectrum are presented for the longshore and offshore sonars. In Fig. 2, these data are combined to produce estimates of the clockwise and counterclockwise (viewed from above) rotary spectra. In both figures the overall motion field is separated into upward and downward (energy) propagating

components. An internal wave convention is assumed here, with downward energy propagation corresponding to upward phase propagation.

In Figs. 1 and 2, the averaging interval increases logarithmically in wavenumber. A logarithmic averaging technique is used for frequency-averaging also. However, additional linear smoothing is employed to reduce the signature of a series of spectral ridges that occur at fixed frequencies. These ridges might be harmonics of the baroclinic tide. They cannot be quantified with adequate statistical precision in this limited, 18-day data set. The linear averaging smoothes them out, allowing a clear view of the underlying continuum. (Whether this "spectral continuum" is strictly an artifact of the severe smoothing remains an issue.)

In Figs. 3 and 4, cross sections of the shear spectrum $\Phi(\kappa, \omega_i)$ are presented as functions of vertical wavenumber at the set of center frequencies $\{\omega_i = 1, 2, 4, 8, 10, 32$ and 64 cpd$\}$. Here linear smoothing is employed in wavenumber. Statistical stability is achieved primarily by averaging in frequency. The frequency averaging interval increases with increasing center frequency.

In Fig. 5 cumulative shear spectra are presented for the 70- and 75-kHz sonars. These are plots of

$$\Phi_i(\kappa) = \int_{1/2f}^{\omega_i} \Phi(\kappa, \omega)d\omega$$

for the set of frequencies $\{\omega_i = 1, 2, 4, 8, 16, 32$ and 64 cpd$\}$. Note that in Fig. 5, the upper limit on the integration band is the same as the center of the averaging bands in Figs. 3 and 4.

In Fig. 6 estimates of the frequency spectrum of shear are presented. These are simply

$$\Phi(\omega) = \int_{\kappa_{min}}^{\kappa_{max}} \Phi(\kappa, \omega)d\kappa.$$

Here $\kappa_{min}$ is taken as 1/530 cpm and $\kappa_{max}$ as 1/28 cpm.

Figure 7 depicts Munk's (1981) inverse Richardson function.

$$\text{Ri}^{-1}(\kappa, \omega_i) = N^{-2} \int_{\kappa_{min}}^{\kappa} \int_{\omega_{min}}^{\omega} \Phi(\hat{\kappa}, \hat{\omega})d\hat{\omega}d\hat{\kappa}.$$

Here $N$ is the Väisälä frequency, $\kappa_{min}$ is $1/530$ m$^{-1}$ and $\omega_{min} = 0.5$ cpd. This is essentially a cumulative shear spectrum, normalized by the Väisälä frequency.

## 3. Discussion: The wavenumber–frequency spectrum of shear

Estimates of the wavenumber–frequency spectrum are presented as defomed surface plots in Figs. 1 and 2 and as series of spectral cross sections in Figs. 3 and 4. The shear variance associated with the spectrum is sensitive to the assumed level of noise contamination. Two estimates of shear variance are given in Table 1. The first includes all forms of measurement noise. The

second estimate is obtained after a modeled noise spectrum is subtracted from the direct estimate of $\Phi(\kappa, \omega)$. These variances are calculated over the vertical-wavenumber band from 1/530 to 1/28 cpm.

The shear spectrum is seen to be band-limited in wavenumber in the region encompassing the inertial and semidiurnal tidal frequencies. Motions of vertical wavelength between 100 and 300 m have the greatest shear spectral density. A pronounced high-wavenumber cutoff is seen in the spectrum, particularly in the near-inertial frequency region. The cutoff occurs over vertical scales of approximately 50 to 80 m. Spectral slopes exceed $\kappa^{-3}$ in this region. The potential influence of FLIP motion on this apparent cutoff is discussed in the Appendix and indicated schematically in Fig. 3.

As frequency increases, the band of most energetic motion shifts to ever higher wavenumbers. At frequencies above 8 cpd only the low-wavenumber side of the energetic band is resolved by the sonar. The wavenumber dependence here appears blue. The wavenumber slope of the high-frequency region is slightly in excess of $\kappa^{+1}$. At very high wavenumber, in excess of 0.03 cpm, a pronounced downturning of the spectrum occurs. This is a manifestation of the finite resolution of the sonar measurements and not a property of the motions in the sea.

The contrast between this estimate of the spectrum and the spectral models proposed by Garrett and Munk (1972, 1975) is clearly seen in Figs. 1–4. Their modeled vertical wavenumber dependence does not change with frequency. Here, the change is striking. On the other hand, Garrett and Munk set out to model the spectrum of a random field of linear internal waves. It is unlikely that all of the motions that contribute variance to this shear spectrum are linear waves.

Support for this contention comes from previous measurements of isotherm vertical motion obtained from the profiling CTD system on FLIP (Occhiello and Pinkel, 1976). Estimates of the wavenumber–frequency spectrum of vertical motion become progressively more red in vertical wavenumber as frequency increases (Pinkel, 1975). This is just the reverse of the trend seen in the Doppler data, which are presumably most strongly influenced by horizontal, not vertical velocity. At frequencies above 1 cph, the spectrum of vertical velocity is dominated by the lowest internal wave mode. The spectrum of slant velocity, in contrast, looks nearly white. If *linear* internal waves are responsible for all of the observed motion, and the wavefield is isotropic, the spectral forms should be congruous. Thus, most of the shear variance on vertical scales less than 60 m comes from the part of the spectrum that is the least wavelike. This casts suspicion on the use of internal wave WKB scaling for the motions in this spectral region.

As a consequence, the convention used in this work, to separate motions into upward and downward propagating components, needs to be reexamined. Specif-
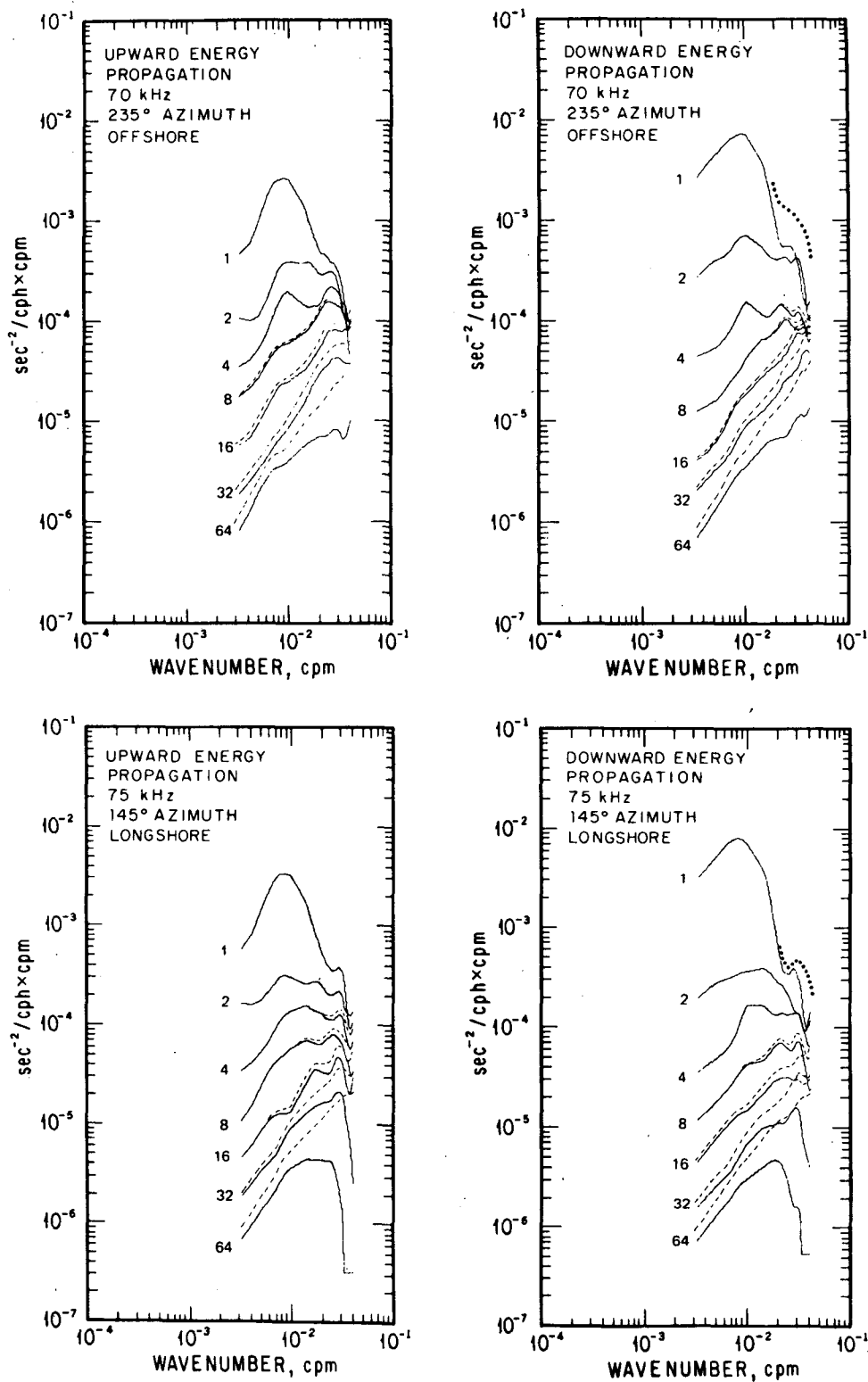
FIG. 3. Cross sections of the component wavenumber-frequency spectrum of shear at 1, 2, 4, 8, 16, 32 and 64 cpd. Spectral estimates are calculated at 20, 36, 68, 132, 260, 516 and 1028 degrees of freedom. Dashed lines give the spectrum as measured. Solid lines give an estimate of the spectrum with a modeled noise spectrum removed. The noise level chosen corresponds to 1.5 cm² s⁻² velocity noise variance. The sharp drop in the spectrum at vertical wavenumbers greater than $3 \times 10^{-2}$ cpm is a consequence of the finite resolution of the measurement. Any actual high-wavenumber cut off of the spectrum is not resolved in these measurements. The dotted modifications to the downward propagating near-inertial cross sections indicate potential corrections to the spectrum to account for FLIP's tilt. For the 70-kHz section an extreme correction was used, corresponding to the ±5° rms tilt (Fig. 9). A more reasonable degree of correction, ±1.5° rms, is applied to the 75-kHz section.
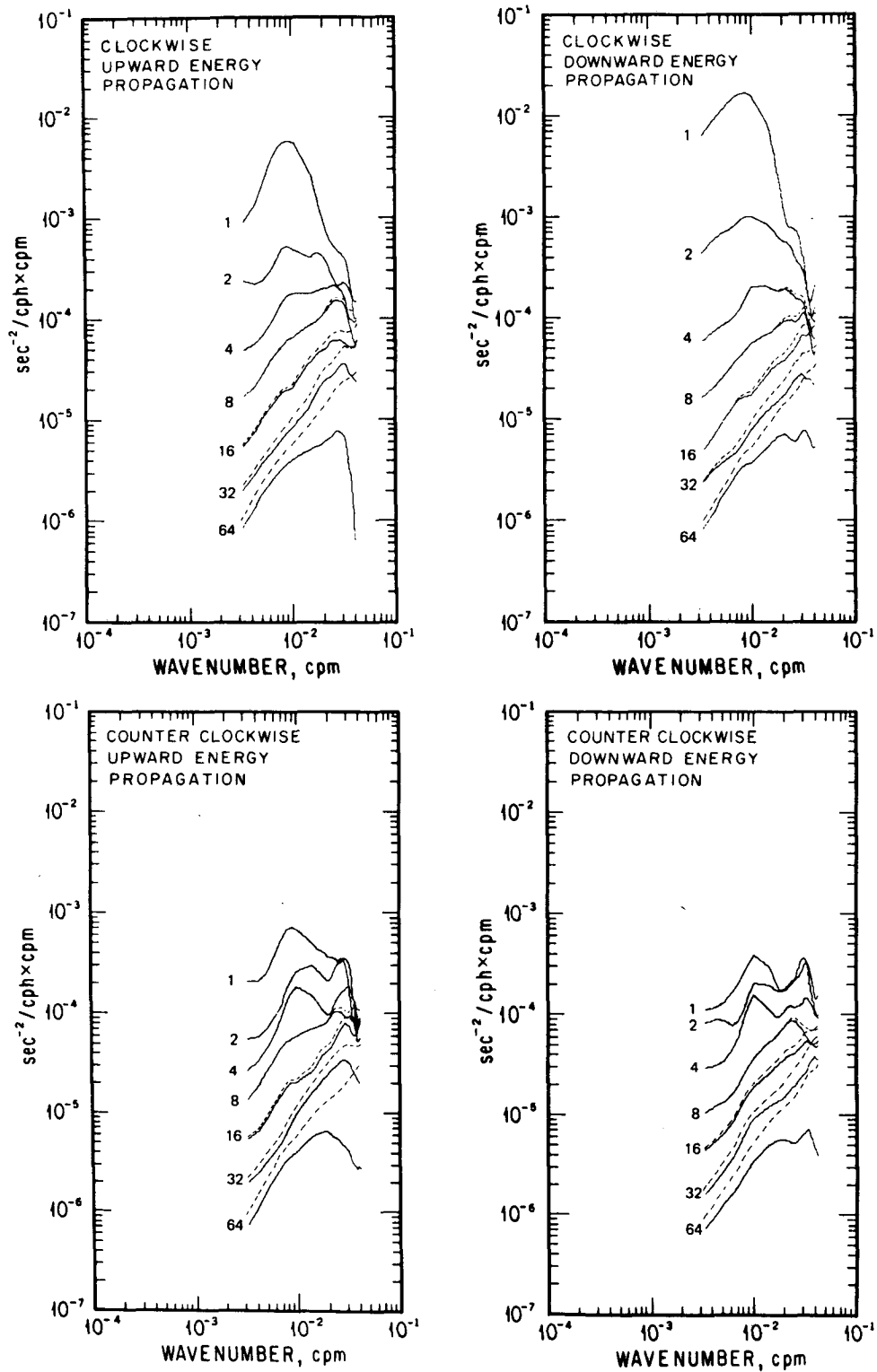
FIG. 4. Cross section of the rotary wavenumber–frequency spectrum of shear.
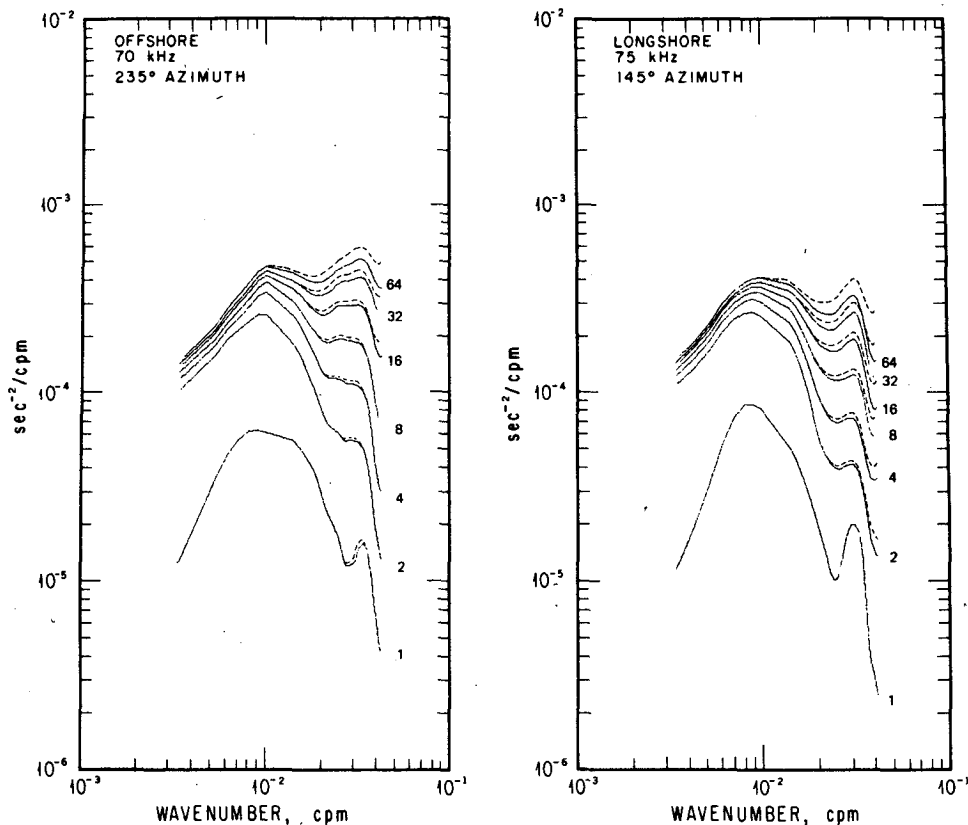The interpretation is as in Fig. 3.

FIG. 5. Cumulative shear variance as a function of vertical wavenumber for the 70- and 75-kHz sonars. The contribution to the overall variance from frequencies 0.5 to 1, 0.5 to 2 · · · 0.5 to 64 cpd is given by the various lines. Dashed lines give the variance contribution as measured. Solid lines show the result of subtracting a modeled noise spectrum. The corresponding velocity noise level assumed is 1.5 cm$^2$ s$^{-2}$. The drop in spectral levels above $3 \times 10^{-2}$ cpm is a consequence of the finite resolution of the measurement.

ically, motions that do not propagate at all will contribute variance equally to the upward and downward spectral estimates. When the up–down spectral levels are examined closely in Figs. 3–4, clear differences are seen at low frequency and intermediate wavenumber, presumably associated with propagating near-inertial waves. At high frequency the up–down symmetry is more apparent.

In contrast, the similarity between the offshore and longshore spectra is nearly perfect at low frequency in the near-inertial band. Even small irregularities in the spectrum are seen to reproduce (Fig. 3). In the tidal (2 cpd) band there is more variance in the offshore record than in the longshore. Curiously, at high frequency the offshore spectral levels are nearly a factor of two higher than the longshore. This is seen in the 16, 32 and 64 cpd cross sections.

## 4. The vertical wavenumber spectrum of shear

The wavenumber–frequency spectrum of shear $\Phi(\kappa, \omega)$ is band-limited in wavenumber at low frequency and blue at high frequency. It would seem difficult to

reconcile this complex variation with the Gargett et al. (1981) view that the wavenumber spectrum $\Phi(\kappa)$ is essentially white at vertical scales between 10 and 100 m. In fact the two-dimensional spectrum estimated here is consistent with a white $\Phi(\kappa)$. This can be seen by integrating $\Phi(\kappa, \omega)$ over frequency, to achieve a wavenumber spectrum alone. This is done in Fig. 5. The frequency integration is performed in a series of one-octave increments, from ½ to 1 cpd, ½ to 2 cpd, ½ to 4 cpd, etc. In this manner the contribution from the various frequency bands to the various wavenumber bands can be seen. The lowest-frequency motions contribute most to the low-wavenumber portion of this spectrum, as expected. However, the contribution to scales less than 50 m comes from progressively higher frequencies. This contrasts with the Garrett–Munk hypothesis that near-inertial motions dominate the contribution to the shear spectrum at all vertical scales. This distinction is of significance in the statistical modeling of low Richardson number events.

It is not surprising that the shear spectrum is not perfectly white over scales of 10–100 m. The long wavelength portion reflects the level of near-inertial
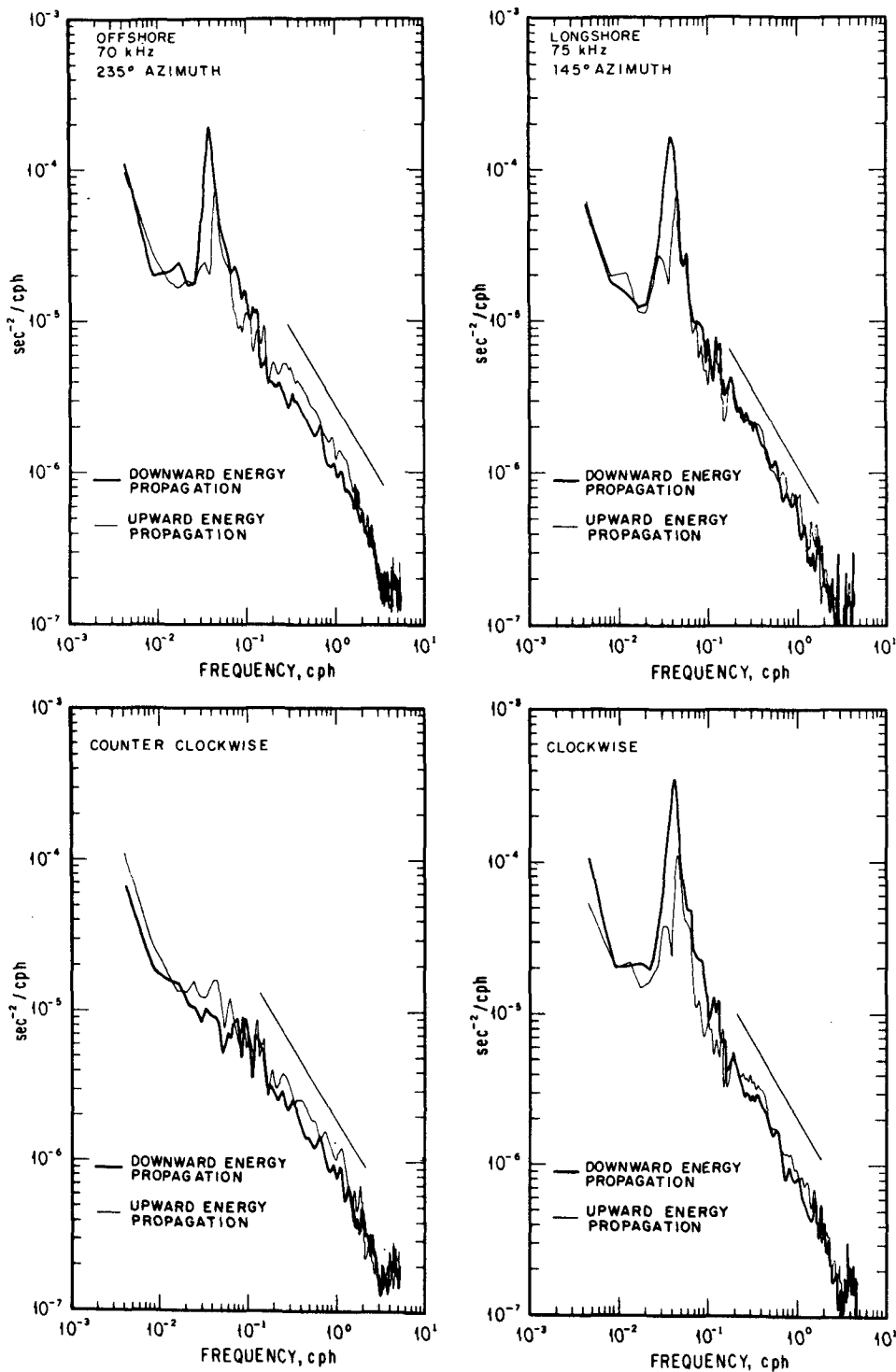
FIG. 6. Component frequency spectrum of shear (top), the rotary frequency spectrum (bottom). The modeled noise spectrum has been removed. An $\omega^{-1}$ reference line is shown.

wave energy, which is known to be highly variable. The shear spectral level at shorter wavelengths, 50–30 m, might well not be due to waves at all. The overall spectral level is approximately a factor of two greater than the Gargett et al. (1981) measurements in the Atlantic.
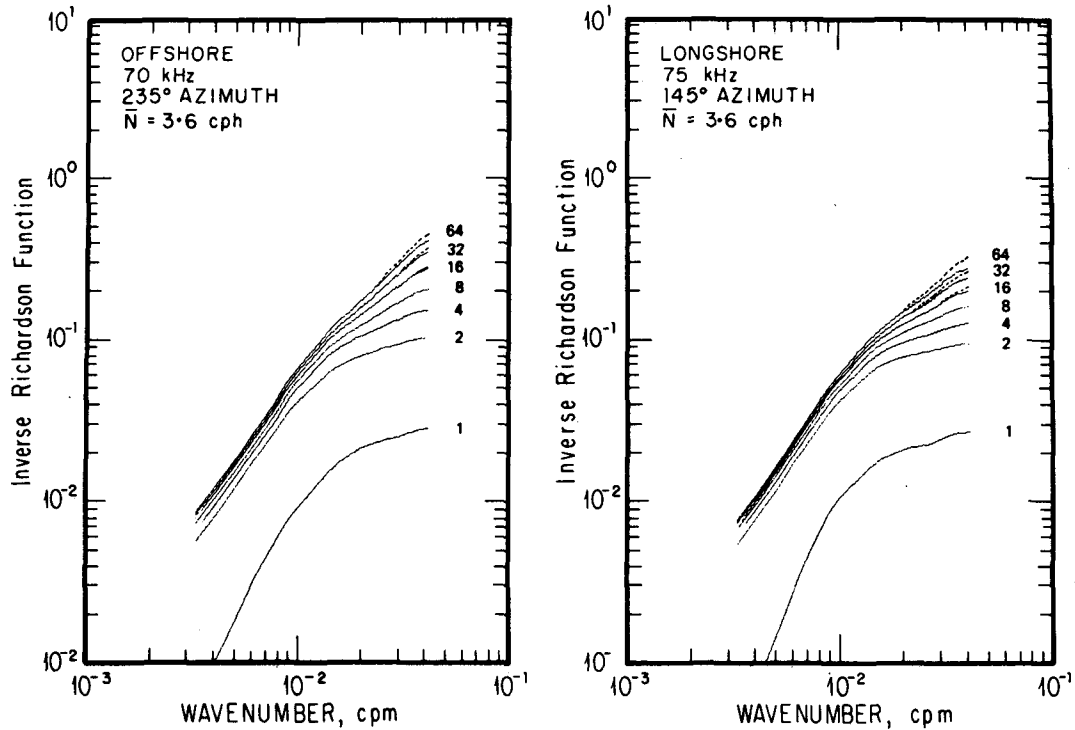
FIG. 7. The inverse Richardson function $Ri^{-1}(\kappa, \omega)$ evaluated at frequencies 1, 2, 4 · · · 64 cpd. The dashed line gives the function with no modeled noise removed. The solid line indicates the result of subtracting a modeled noise spectrum from the shear spectral estimate.

## 5. The frequency spectrum of shear

The wavenumber–frequency spectrum $\Phi(\kappa, \omega)$ can also be integrated over wavenumber to produce a frequency spectrum of the shear field (Fig. 6). Here frequency spectra are presented for offshore and longshore velocity components as well as for clockwise and counterclockwise rotating motions. The contributions to these spectra from upward and downward propagating motions are presented separately. The spectral esti-

mates are formed from $\Phi(\kappa, \omega)$ by integrating in $\kappa$ over 50 wavenumber bands (25 independent bands) and then smoothing additionally in frequency. Band-averaging over 10 bands (above 0.16 cph) and over 20 bands (above 0.32 cph) was employed. Adjacent frequency bands are not independent.

The spectra have a nearly $\omega^{-1}$ form from 0.1 to 1 cph. A hint of a Väisälä cutoff is seen at 3 cph. Above this frequency the spectra drop to an irregular noise floor of order $1.5 \times 10^{-7}$ s$^{-2}$/cph. The spectral form

TABLE 1. Shear variance (s$^{-2}$ × 10$^6$) for seven one-octave frequency bands from 0.5 to 64 cpd. Vertical propagation direction is determined using an internal wave convention. "Downward" implies downward propagation energy or upward phase propagation. The left number in each column gives the variance from the uncorrected spectral estimate. The right number gives the variance from a spectral estimate with a modeled noise spectrum removed. The modeled noise level corresponds to 1.5 cm$^2$ s$^{-2}$ of (slant) velocity noise.

| Frequency (cpd) | Offshore 70 kHz 235° Azimuth | | Alongshore 75 kHz 145° Azimuth | |
|---|---|---|---|---|
| | Downward | Upward | Downward | Upward |
| 0.5–1 | 0.71, 0.71 | 0.38, 0.38 | 0.72, 0.72 | 0.37, 0.37 |
| 1–2 | 1.73, 1.72 | 1.19, 1.18 | 1.58, 1.57 | 1.20, 1.19 |
| 2–4 | 1.00, 0.99 | 0.90, 0.88 | 0.70, 0.68 | 0.53, 0.51 |
| 4–8 | 0.82, 0.79 | 1.12, 1.08 | 0.72, 0.68 | 0.72, 0.69 |
| 8–16 | 1.10, 1.03 | 1.43, 1.36 | 0.78, 0.70 | 0.83, 0.75 |
| 16–32 | 1.12, 0.97 | 1.47, 1.32 | 0.84, 0.69 | 0.94, 0.80 |
| 32–64 | 1.26, 0.96 | 1.35, 1.05 | 0.94, 0.64 | 0.97, 0.67 |
| Total | 7.75, 7.16 | 7.83, 7.24 | 6.27, 5.68 | 5.56, 4.97 |

above 2 cph is strongly influenced by the modeled "noise removal" employed. When no noise is "removed", the 3 cph cutoff becomes less distinct and the high-frequency noise level doubles, to approximately $3 \times 10^{-7}$ s$^{-2}$/cph.

The $\omega^{-1}$ slope at intermediate frequency contrasts with an $\omega^{-1.5}$ slope seen in the corresponding spectrum of velocity (Pinkel, 1984). The difference in slopes results from the changing form of the wavenumber dependence of the spectrum with changing frequency.

Pronounced near-inertial peaks dominate the offshore and longshore spectra, as well as the clockwise rotary spectrum. Near-inertial shear variance associated with downward propagating wave groups exceeds that of upward propagating groups. Surprisingly, upward propagating shear levels are found to be significantly greater than downward over the frequency range 0.2–2 cph for the offshore (but not longshore) measurements. This is seen in the velocity spectra also (Pinkel, 1984).

## 6. The inverse Richardson function

Munk (1981) introduced the inverse Richardson function,

$$\text{Ri}^{-1}(\kappa) = N^{-2} \int_0^\kappa \Phi(\hat{\kappa})d\hat{\kappa}$$

as a means of quantifying the contribution of shear variance to the Richardson number as a function of vertical scale. The white shear spectrum of Gargett et al. (1981) imply a $\kappa^{+1}$ form for the inverse Richardson function. Here, the definition of the inverse Richardson function can be broadened to include the effects of both wavenumber and frequency variation in $\Phi(\kappa, \omega)$.

$$\text{Ri}^{-1}(\kappa, \omega) = N^{-2} \int_{\kappa_{\min}}^\kappa \int_{\omega_{\min}}^\omega \Phi(\hat{\kappa}, \hat{\omega})d\hat{\omega}d\hat{\kappa}$$

where $\omega_{\min} = 0.5$ cpd and $\kappa_{\min} = 1/530$ cpm.

The level of Ri$^{-1}$ is somewhat arbitrary in that the proper value of $N^2$ is difficult to define. A WKB stretching appropriate for internal waves is used to calculate $\Phi(\kappa, \omega)$. Yet much of the high frequency shear might not be due to internal waves. Should the value of $N^2$ be determined by averaging over the actual depth of the observations or over the WKB stretched depth? If stretched depth is used, the higher values of $N$ are more heavily weighted in the average. The value of $N$ = 3.6 cph was chosen, subjectively, for the present calculation. It is closer to the value averaged over stretched rather than real depth.

Profiles of the Ri$^{-1}(\kappa, \omega)$ as a function of wavenumber at fixed frequencies are presented in Fig. 7. The low-frequency profiles, 0.5–1 cpd and 0.5–2 cpd, increase rapidly with increasing $\kappa$, but then level off considerably at $\kappa > 0.02$, vertical scales shorter than 50 m. This reflects the low level of shear spectral density at

high wavenumber (above the wavenumber cutoff) relative to that below. Note that most of the "near-inertial" shear occurs at frequencies slightly above 1 cpd. This is responsible for the large separation between the 1 and 2 cpd profiles. As the contribution of higher frequencies is included, there is virtually no change in the form of Ri$^{-1}(\kappa, \omega)$ at low wavenumber. This is a consequence of the dominance of near-inertial shears at low wavenumber. At high wavenumber, the high-frequency contribution of shear variance significantly increases the inverse Richardson function.

Gargett et al. (1981) emphasize the importance of the value of Ri$^{-1}(\kappa, \omega_{\max})$ at the vertical transition scale of 10 m. They suggest a value of Ri$^{-1}(0.1, \omega_{\max}) = 1$ is universal. If the present estimates of Ri$^{-1}(\kappa, \omega_{\max})$ are extrapolated to 10 m scale, values of 1.25 and 0.6 are obtained for the offshore and longshore data respectively. This corresponds to component Richardson numbers of 0.8 and 1.6. When the results are combined to give an estimate of the Richardson number reflecting both components of the shear an overall extrapolated value of 0.540 is obtained. It is unlikely that the estimate of $N^2$ is a factor of two in error. The disagreement between this result and the Gargett et al. universal (but only measured once) value stems primarily from the unusually large shears associated with a few distinct near-inertial wave packets that propagated under FLIP during the course of the experiment. The shear spectral levels (Fig. 5) are a factor of two greater than those of Gargett et al. It is not surprising that the inverse Richardson function should be a factor of two greater. However, the extrapolation of these data from 30 m vertical scale down to 10 m is a highly uncertain procedure. The blue regions of $\Phi(\kappa, \omega)$ must eventually level off with increasing wavenumber, and then decrease, in order to be consistent with the Gargett et al. (1981) measurements between 10 and 1 m scales.

## 7. Concluding discussion

An estimate of the vertical wavenumber spectrum of shear, $\Phi(\kappa, \omega)$ has been presented. The estimate differs from previous expectation in that the wavenumber dependence is band-limited at low frequency and blue at high. It is emphasized that this unusual form is completely consistent with previous measurements of the one-dimensional shear spectrum $\Phi(\kappa)$, which are nearly white (Gargett et al., 1981). A cutoff in $\Phi(\kappa, \omega)$ as a function of wavenumber is seen at low frequency. Little indication of this cutoff is seen in $\Phi(\kappa)$. It is obscured by the shear-variance contribution from high wavenumber and high frequency. This high wavenumber-high frequency shear is unlikely due to linear internal waves. Previous estimates of the spectrum of isotherm vertical displacement (Pinkel, 1975) indicate a spectrum that becomes increasingly dominated by low modes (long vertical wavelengths) as frequency in-

creases. This shear spectral estimate suggests the reverse trend.

An estimate of the vertical displacement spectrum is currently being prepared from a sequence of six thousand CTD profiles obtained in May 1980, concurrent with the sonar measurements. From the difference between the measured shear spectrum and that part that would be predicted, using linear internal wave theory, from the displacement spectrum, the wavenumber–frequency distribution of the disparity can be calculated. In advance of this difficult exercise, one can conjecture that the shear spectrum of the high-frequency field is band-limited in wavenumber, rising as $\kappa^1$ for $\kappa \ll \kappa_0$ (as seen in the high-frequency cross section of Figs. 3–4) and falling as $\kappa^{-1}$ for $\kappa > \kappa_0$ as estimated by Gargett et al. (1981). Here $\kappa_0$ is some wavenumber, suggested to be 0.1 cpm by Gargett et al. (1981), that is too large to be resolved by the Doppler sonars.

Holloway (1983) has suggested that the high frequency–high wavenumber shear consists of a mixture of nonlinear internal waves of short horizontal wavelength and "two-dimensional geostrophic turbulence," advected to high encounter frequency by the large-scale and internal-wave fields. He refers to the possibility of nonlinear interaction between fields associated with the "geostrophic branch" and internal-wave branches of a total dispersion surface. Recently Müller (1985) has coined the term "Vortical Mode" in his study of the two-dimensional motions. He identifies this class of motions as responsible for the disparity between estimates of the vertical coherence of vertical motion vs horizontal motion in the IWEX data set. (Müller et al., 1978).

These dynamic models of the high frequency–high wavenumber shear must be reconciled with the rather elaborate arguments offered by Gargett et al. (1981) in explaining their spectral estimate $\Phi(\kappa)$. They assert that, over the range of vertical scales between 1 and 10 m, the shear spectrum is completely determined by the two parameters $\epsilon$ and $N$. Here $\epsilon$ is the rate of turbulent dissipation. The shear spectral level is set by

$$\Phi_b \equiv (\epsilon N)^{1/2}.$$

A buoyancy scale is defined by

$$\kappa_b = (N^3/\epsilon)^{1/2}.$$

They find empirically that the spectrum has a $\kappa^{-1}$ form at wavenumbers less than $\kappa_b$ down to some $\kappa_0$. Curiously, if one states this explicitly,

$$\Phi(\kappa) = \frac{\kappa_b}{\kappa} \Phi_b, \quad \kappa_0 < \kappa < \kappa_b$$

$$= (\epsilon N)^{1/2}(N^3/\epsilon)^{1/2}\kappa^{-1}$$

$$= N^2\kappa^{-1}, \quad \kappa_0 < \kappa < \kappa_b.$$

It is seen that the spectral level in this region is independent of $\epsilon$. Now, if this regime is valid down to some wavenumber $\kappa_0$, below which the spectrum is of constant level,

$$\Phi(\kappa) = \Phi_0, \quad \kappa < \kappa_0$$

then $\Phi_0 = N^2/\kappa_0$. As a consequence, the inverse Richardson function, evaluated at $\kappa_0$, is always of order 1, independent of $N^2$, $\epsilon$, $\kappa_0$, and the dynamics of the region $\kappa < \kappa_0$.

$$\mathrm{Ri}^{-1}(\kappa_0) = \Phi_0\kappa_0 N^{-2} \equiv 1.$$

Their argument can be continued a second step if one truly believes that the shear spectrum $\Phi(\kappa)$ is constant at wavenumbers below $\kappa_0$, that its value is globally universal, and that it varies in the vertical according to WKB internal-wave scaling, $[\Phi(\kappa, z) \sim N^2(z)]$. Then $\kappa_0 = N^2/\Phi_0$ is a universal dimensional constant independent of both depth and location. Gargett et al. (1981) find $\kappa_0^{-1}$ approximately 10 m. In these observations, $\kappa_0^{-1} \approx 25$ m.

However, if the small-scale shear is not due to internal waves, the applicability of WKB scaling is questionable. In addition, since the shear field is dominated by internal wave motions at vertical scales longer than 60 m and (perhaps) nonwave motions at shorter scales, is there a reason why the overall shear spectrum is nearly white? Similarly, the relationship between the strongly horizontal nonwave field and the yet smaller-scale motions, successfully scaled with $\epsilon$ and $N$, remains to be explained.

## APPENDIX

### Sonar Geometry, Resolution and FLIP Tilt

For the purpose of studying shear, one would like data in the form of continuous vertical profiles of horizontal velocity. The FLIP sonars provide slant profiles of slant velocity. Linear internal wave theory suggests that these measurements are a good approximation to the ideal at frequencies much less than $N$. However, the derivative with range of slant velocity will more closely approximate $\partial w/\partial x$ than $\partial u/\partial z$ at frequencies near $N$. Could this geometric effect be responsible for

the changing form of the spectrum with frequency? The measurement process is simulated in the first section below, using the Garrett–Munk 1975 spectrum. It is found that the complex geometry plays little role in determining the observed spectral form.

More significant effects result from the tilting of FLIP by waves and by wind gusts. Tilting not only degrades the vertical resolution of the measurements but confuses the depth and time dependence of the motions as well. The vertical resolution issue is discussed in the second section below. An investigation of tilt and the depth/time dependence concludes the Appendix.

## 1. The shear spectrum and sonar beam geometry

The slant wavenumber–frequency spectrum sensed by a sonar can be related to the true horizontal wavenumber–frequency spectrum by a rather complicated integral [Pinkel, 1981, Eqn. (10)]. Many of the weighting terms in this integral are frequency dependent. To see whether the frequency dependence observed in these spectral estimates is purely an effect of the observation, one can evaluate the integral using a model form for the horizontal wavenumber–frequency spectrum. The Garrett–Munk (1975) spectrum model is attractive to use, as its wavenumber dependence does not change with frequency. The spectrum is also assumed to be horizontally isotropic and vertically symmetric. The signature of the wave components on the sonar velocity measurement will vary significantly, however, depending on the propagation direction of the waves relative to the sonar beam direction. The modal cutoff is set at $j^* = 6$ (6 cycles per buoyancy scale depth), corresponding to 12–18 "equivalent modes".

Synthetic estimates of a slant wavenumber–frequency spectrum of velocity are generated at frequencies of $1.1f$ ($f$ is singular), $2f$, $4f$, . . . , $64f$ in Fig. 8 left. The spectrum is evaluated at slant wavenumbers 1 through 30 cycles/slant kilometer. A companion spectrum of the slant difference of slant velocity (i.e., shear) is presented in Fig. 8 right. In neither spectrum is there a significant variation in the wavenumber dependence with frequency. The interesting effect is the nearly identical spectral values at frequencies of 32 and 64 cpd. At these high frequencies, the sonar is sensing predominantly the vertical component of velocity. As the spectrum of vertical velocity does not change with frequency, the successive profiles are congruent.

## 2. Resolution and high-frequency tilt

In the absence of time-dependent tilting of FLIP, the effective depth resolution of these measurements is set by the combined effect of the vertical beamwidth of the sonar beams and the range resolution along the beams. The effective range resolution here is approximately 40 m (depth resolution 28 m). The resolution

is set by the duration of the transmitted acoustic pulse as well as subsequent averaging of the data in range. The vertical beam widths of the sonars are less than 1°.

Acoustic pulses are transmitted at nominal two-second intervals. However, the autovariance function of the returns is averaged over five-minute intervals to improve the statistical stability of the Doppler velocity estimate. During this time surface waves are causing FLIP to rock. Direct forcing at the wave frequency as well as a high-tilt response at a 1-minute tilt resonance period result in rms tilts of 2° in rough seas. Peak tilts of ±5° are occasionally seen. The effective beamwidth of the array is thus much wider than the nominal value. It is given by the convolution of the nominal beamwidth with the tilt probability density function over the five-minute averaging interval. This renders the vertical resolution of the array both weather and depth dependent, as $\Delta z = r\Delta\theta$. Note that the smearing effects of tilt are most significant at great range depth.

To model these effects, WKB solutions to the internal wave equation

$$W''_{(z)} + k_H^2 \left( \frac{N^2 - \omega^2}{\omega^2 - f^2} \right) W_{(z)} = 0$$

were generated numerically using a modeled Väisälä profile:

$$N(z) = N_0 e^{-z/b}, \quad b = 800 \text{ m}.$$

Solutions were obtained in the midfrequency limit $f^2 < \omega^2 < N^2$ at values of $k_H/\omega$ such that the average vertical wavenumber was $0.01, 0.02, 0.03, . . .$ cpm over the depth interval 100 to 650 m. Note that at great depth, the local vertical wavelength is somewhat longer than the average, at shallow depth it is somewhat shorter. This partially mitigates the increasing effect of tilt smearing with range.

From these solutions for vertical velocity, the corresponding set of solutions for horizontal velocity were generated. Their variance, over the depth range 100–650 m, was calculated. The solutions were subsequently smoothed by averaging over "range cells" whose dimensions, while fixed in range and in angle, actually increase in the depth dimension with increasing range. The range bins are weighted in range by a triangle function with a 40-m base. This approximates a rectangular resolution cell of 22 m (resulting from a 30 ms acoustic pulse), which is subsequently range-averaged over an additional 20 m. The angular width of the range bin is determined in both "optimistic" and "realistic" cases. In the optimistic case, a $sinc^2$ function is used. This closely approximates the angular dependence of the acoustic beam. In the realistic case, a Gaussian angular dependence is used. This more closely approximates the distribution of angles in which the narrow beam was pointed during the five-minute time-averaging interval.
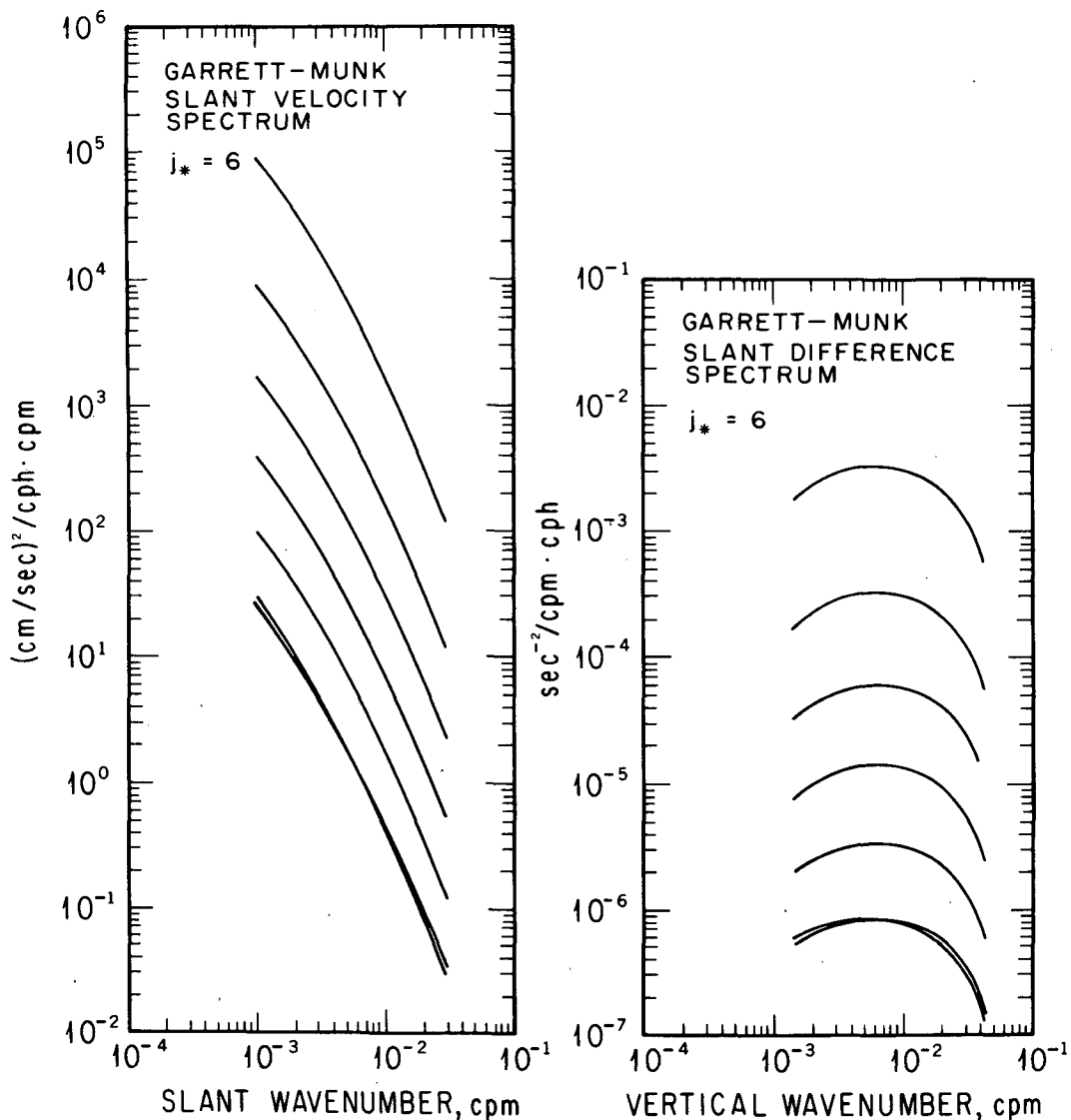
FIG. 8. A simulated slant-wavenumber spectrum of slant velocity, as seen by a sonar beam directed 45° downward from horizontal (left). The corresponding spectrum of shear as a function of effective vertical wavenumber (right). Cross sections are presented at frequencies of 1.1, 2, 4, 8, . . . , 64 cpd. The Garrett–Munk 1975 spectrum is used as a basis for this simulation, with a 1 cpd inertial frequency assumed.

Range-bin dimensions are calculated as a function of depth for a variety of assumed angular beam widths, corresponding to different degrees of rms tilt. The horizontal velocity wavefunctions are averaged over the range-cell volumes and the variance of the spatially averaged velocity values is recalculated. The ratio of the variance of the averaged velocity to the un-averaged is plotted in Fig. 9 as a function of the WKB average vertical wavenumber. At low wavenumber, the volume averaging has little effect on the observed variance. In the "optimistic" case, with an angular width given by the sonar beamwidth, the variance is seen to be reduced to 80% of its true value at vertical scales of 30 m. This is an insignificant effect. However, when tilting is realistically assessed, the variance can be brought to half its true value at 30-m scale, and to 30% of the true value at 20-m scale, for large values of rms tilt. In retrospect, its is attractive to identify the sharp downturning of the spectra with wavenumber, visible at high wavenumber in Figs. 3–5, with a tilt induced degradation of vertical resolution. Fortunately, one can see from Fig. 9 that the correction to the form of the spectrum over the interesting range of scales between 100 and 30 m is most likely rather slight. The actual correction is indicated by dotted lines in Fig. 3 for the downward propagating near-inertial bands.
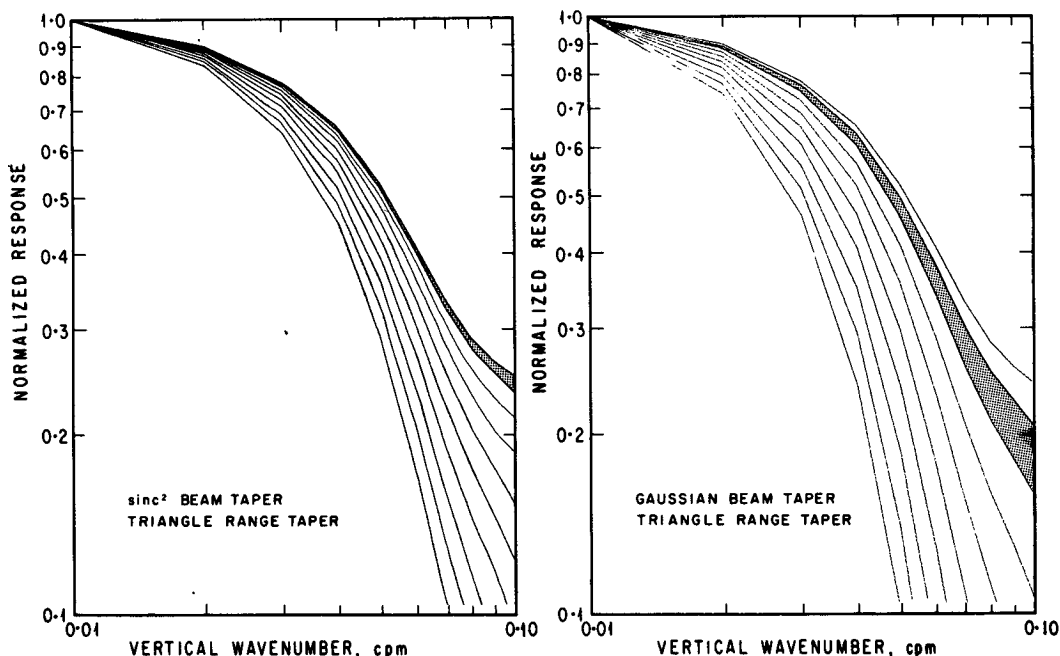
FIG. 9. Wavenumber spectral response as a function of assumed vertical beamwidth. A sinc$^2$ beam shape is assumed in the left display. Response is given for widths of $\pm0.5°$ (top) through $\pm5°$ (bottom), where beamwidth is measured to the first zero of the sinc$^2$ function. The right plot gives the response for an assumed Gaussian beam shape. Response curves are given for beam widths $\pm0.5°$ to $\pm5°$ between $e^{-1}$ points on the Gaussian. Shaded regions indicate the most likely response in perfectly calm conditions (left), due to the finite sonar beam width and in moderate conditions (right), due to FLIP motion.

## 3. Tilt and depth/time dependence

In the analysis of this data set, time series of shear are formed at fixed range. If FLIPs tilt changes slowly over the minutes to days of the time series, depth variations in shear will appear as time variations at fixed range.

Fortunately, there is a distinct geometric signature associated with this form of "fine structure" contamination, even when the shear field is random. This can be seen when a Fourier model of the shear is employed:

$$s(r, t) = \int_{-\infty}^{\infty} \int_{-\infty}^{\infty} A(\kappa, \omega)e^{i[\kappa r\cos\theta(t)-\omega t]}d\kappa d\omega.$$

Here $r$ is sonar range, $\theta(t)$ is the angle of the sonar beam from vertical and $\kappa$ is the vertical wavenumber. In 1980 $\theta(t) = 45° + \delta(t)$, where $\delta$ is the time variable part of the tilt, which was not measured. Subsequent measurements of low-frequency tilt, made when FLIP was loaded comparably to the 1980 experiment, show that it is surprisingly small, less than 0.5° rms except in periods of extreme wind. However, even this small tilt variation causes significant vertical excursion of the sonar beams at great range. The resulting time-variation dependence of the shear at fixed sonar range is given by

$$\frac{\partial s}{\partial t} = -ir\sin\theta\,\frac{d\theta}{dt}\int_{-\infty}^{\infty}\int_{-\infty}^{\infty}\kappa Ae^{i(\kappa r\cos\theta-\omega t)}d\kappa d\omega$$

$$-i\int_{-\infty}^{\infty}\int_{-\infty}^{\infty}\omega Ae^{i(\kappa r\cos\theta-\omega t)}d\kappa d\omega.$$

The effect of tilt variation is given by the first term on the right while the intrinsic time variation is given by the second. Note that the magnitude of the contamination increases linearly in range. It also increases with wavenumber, provided the wavenumber dependence of $A(\kappa, \omega)$ is $\kappa^{-1}$ or "whiter". One can form a quantity that formally separates the noise and signal by noting

$$\frac{\partial s/\partial t}{\partial s/\partial r} = -r\tan\theta\,\frac{d\theta}{dt} - \frac{\int_{-\infty}^{\infty}\int_{-\infty}^{\infty}\omega Ae^{i(\kappa r\cos\theta-\omega t)}d\kappa d\omega}{\cos\theta\int_{-\infty}^{\infty}\int_{-\infty}^{\infty}\kappa Ae^{i(\kappa r\cos\theta-\omega t)}d\kappa d\omega}$$

$$= -r\tan\theta\,\frac{d\theta}{dt} + \left(\frac{\partial s}{\partial t}\bigg/\frac{\partial s}{\partial r}\right)_{\text{uncontaminated}}.$$

The contamination term in this ratio increases linearly and has no phase reversals with range. Random fluctuations of the ratio with range should be due to the true signal variation.

In Fig. 10 top, a 40-hour segment of shear is plotted as a function of range and time. There are several clear
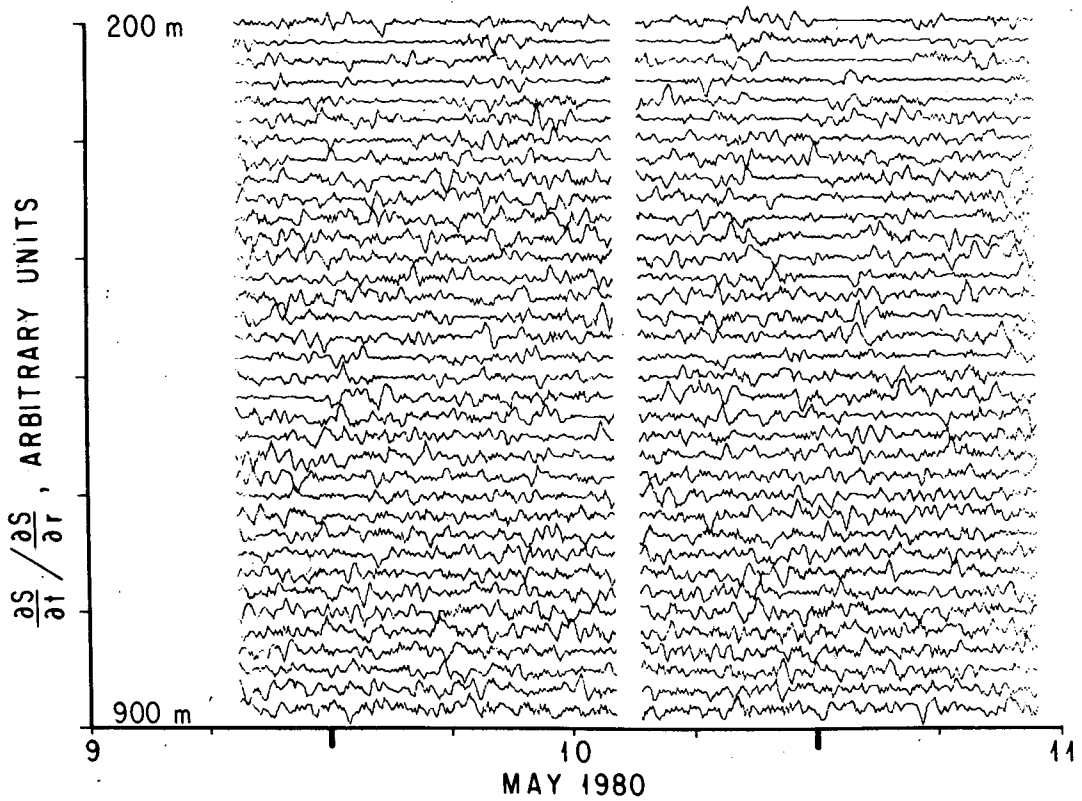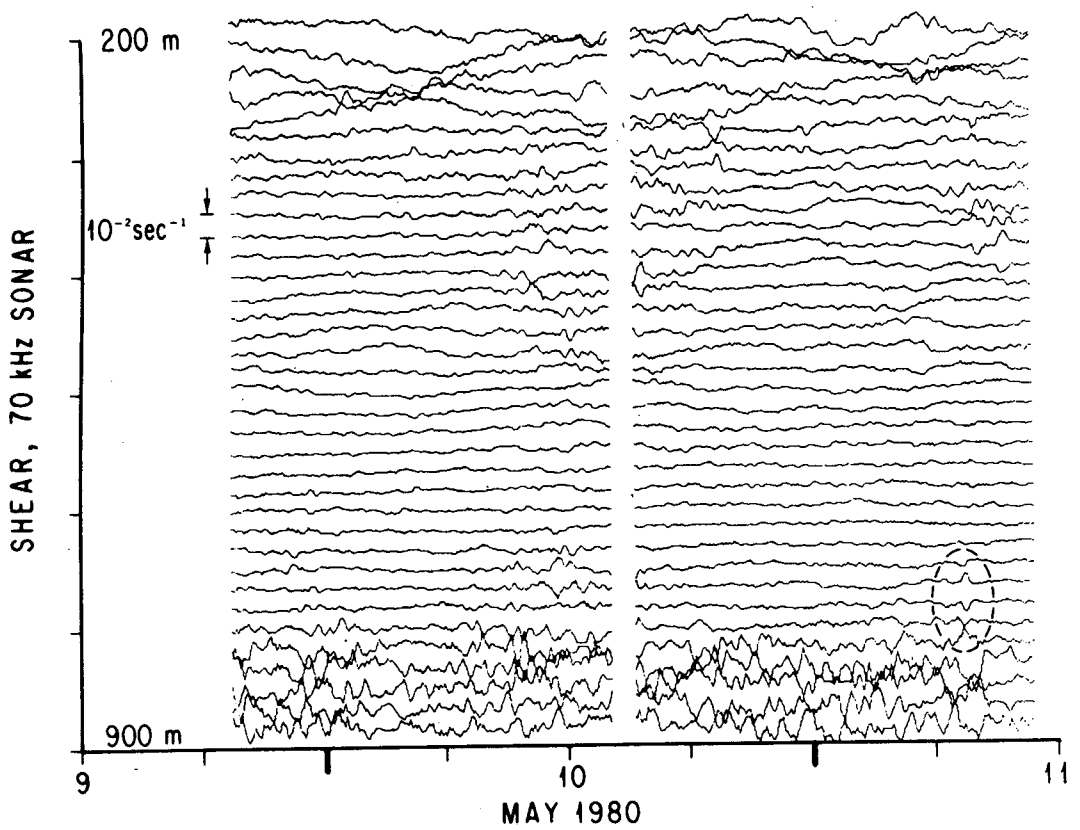
FIG. 10. A 40-hour sample of the shear field plotted as time series at successive slant ranges from 200 to 900 m (top). An isolated spike in the Doppler velocity estimates will result in a symmetric pair of shear disturbances (exampled circled). The ratio $(\partial s/\partial t)/(\partial s/\partial r)$ for this section of data (bottom).

episodes of high frequency–high wavenumber activity at intermediate range. These die out at great range as suggested by linear internal wave scaling, rather than grow, as the noise model would predict. Note that the shear does not appear to consist of a collection of "frozen" low-frequency features that appear first at one range, then at another, as FLIP tilts. The extremely noisy appearance of the bottom five ranges is due to weak sonar returns from great range, and not tilt. Figure 10 bottom shows the corresponding ratio

$$\frac{\partial s/\partial t}{\partial s/\partial r}.$$

The random nature of the field is clearly evident. One concludes that while tilt errors are present in these data, their effect does not dominate the intrinsic variability.

## REFERENCES

Gargett, A. E., P. J. Hendricks, T. B. Sanford, T. R. Osborn and A. J. Williams, 1981: A composite spectrum of shear in the upper ocean. *J. Phys. Oceanogr.,* **11,** 1258–1271.

Garrett, C. J. R., and W. H. Munk, 1972: Space-time scales of internal waves. *Geophys. Fluid Dyn.,* **2,** 225–264.

——, and ——, 1975: Space-time scales of internal waves, a progress report. *J. Geophys. Res.,* **80,** 291–297.

——, and ——, 1979: Internal waves in the ocean. *Annual Review of Fluid Mechanics,* Vol. 11, Annual Reviews, 291–369.

Holloway, G., 1983: A conjecture relating oceanic internal waves and small scale processes. *Atmos. Ocean,* **21,** 107–122.

Müller, P., 1985: On current finestructure and vortical motions. *J. Phys. Oceanogr.,* (submitted).

——, D. J. Olbers and J. Willebrand, 1978: The IWEX spectrum. *J. Geophys. Res.,* **83,** 479–500.

Munk, W. H., 1981: Internal waves and small scale processes. *Evolution of Physical Oceanography,* MIT Press, 264–290.

Occhiello, L. M., and R. Pinkel, 1976: Temperature measurement array for internal wave observation. *MTS-IEEE Oceans '76,* 20E1–20E7.

Pinkel, R., 1975: Upper ocean internal wave observation from FLIP. *J. Geophys. Res.,* **80,** 3892–3910.

——, 1981: On the use of Doppler sonar for internal wave measurement. *Deep-Sea Res.,* **28A,** 269–289.

——, 1983: Doppler sonar observations of internal waves: wavefield structure. *J. Phys. Oceanogr.,* **13,** 805–815.

——, 1984: Doppler sonar observations of internal waves: The wavenumber frequency spectrum. *J. Phys. Oceanogr.,* **14,** 1249–1270.